Spectroscopy of Rb atoms in hollow-core fibers

Aaron D. Slepkov,* Amar R. Bhagwat, Vivek Venkataraman, Pablo Londero, and Alexander L. Gaeta
School of Applied and Engineering Physics, Cornell University, Ithaca, New York 14853, USA
(Received 20 January 2010; published 18 May 2010)

Recent demonstrations of light-matter interactions with atoms and molecules confined to hollow waveguides offer great promise for ultralow-light-level applications. The use of waveguides allows for tight optical confinement over interaction lengths much greater than what could be achieved in bulk geometries. However, the combination of strong atom-photon interactions and nonuniformity of guided light modes gives rise to spectroscopic features that must be understood in order to take full advantage of the properties of such systems. We use light-induced atomic desorption to generate an optically dense Rb vapor at room temperature inside a hollow-core photonic band-gap fiber. Saturable-absorption spectroscopy and passive slow-light experiments reveal large ac Stark shifts, power broadening, and transit-time broadening, that are present in this system even at nanowatt powers.

DOI: 10.1103/PhysRevA.81.053825 PACS number(s): 32.70.Jz, 42.50.Gy, 42.70.Qs, 42.65.Wi

I. INTRODUCTION

Recently, there have been significant advances in ultralow-light level linear and nonlinear light-matter interactions with hot molecular gases and atomic vapors [1–6]. The main applications driving these efforts include gas sensing [7,8], frequency stabilization [9–11], single- and few-photon nonlinear optical switching [1,2,12,13], and slow light and pulse storage [14,15]. Over the past few years, several approaches have been identified for achieving strong light-matter interactions in confined micro- and nanoscaled geometries. These include photonic interactions with atoms [1,2,16,17] and molecules [3,4,18–21] loaded into hollow-core photonic band-gap fibers and hollow semiconductor waveguides [5,22], and evanescent interactions with species surrounding nanoscale semiconductor waveguides [23], tapered optical fibers (TOF) [6,24], microcavities [25,26], and high-Q optical microresonators [27,28]. The primary motivation of these approaches is to increase the strength of the photonic interactions by maximizing the intensity of the light mode and the interaction length. Hollow waveguide geometries provide for the joint confinement of the light and the atomic or molecular gas of interest in the same physically bounded photonic structure for lengths that can be several orders of magnitude larger than those in conventional bulk focusing geometries [29]. As a result, a significant and growing body of recent work has been dedicated to the study of the spectroscopy [18–21,30,31], nonlinear optical applications [2,4,16,17,32], and gas sensing [8] of atoms and molecules confined to the hollow core of microstructured fibers. Recent reports primarily describe the use of acetylene gas [4,18,20,33] and rubidium vapor [1,2,17,31,34,35], but also include methane [8], hydrogen cyanide [19], ammonia [21], hydrogen [3], and xenon [16]. The utility of hollow semiconductor waveguides, such as that recently demonstrated in hollow 5 μm $\times$ 12 μm cross-sectional ARROW waveguides [5,22] offers similar advantages, with the added potential for monolithic integration with Si-based photonic circuits. In the case of evanescent interactions [36], light is most often bound to photonic structures in which the guided mode extends slightly beyond the physical structure, where it can interact with surrounding atoms, molecules, or particles. To achieve this interaction, the photonic structures must be extremely small (on the order of the wavelength of light), and, thus, the evanescent intensities can be sufficiently high as to provide strong nonlinear optical effects [37]. Although in this case, the matter is not confined to the waveguide structure, the interaction region is well defined and confined to within 1 μm of the photonic-device surface. These geometries can, thus, represent an even tighter confinement than in co-confined waveguide geometries.

Clearly, the promise of ultralow-power nonlinear optics makes photon-atom interactions in waveguiding geometries an active and exciting area of research. However, the very nature of these geometries introduces a number of other effects—often undesirable—that pose challenges for applications and interpretations of spectroscopic data: First, the agile loading of atoms and molecules into hollow waveguides often encounters a significant difficulty: Gas kinetics limit the speed with which, for example, hollow-core photonic band-gap fibers (HC-PBGFs) can be pressurized and can be evacuated [38]. Furthermore, significant linewidth broadening of the hot vapors and gases confined to micrometer- and nanometer-length scales is unavoidable. Early studies of acetylene [4] and Rb [17] confined in hollow-core fiber identified collisions with the core walls as the primary broadening mechanism. This effect is inherently connected to transit-time broadening in such systems, and the two are often grouped together. Furthermore, effects such as electromagnetically induced transparency (EIT) [39] that rely on long-lived coherences between closely spaced hyperfine energy levels will experience significant ground-state decoherence if collisions with the walls lead to incoherent population mixing [40]. This broadening is equal to the rate of collisions with the walls, and, thus, scales inversely with the diameter of the waveguide and is directly proportional to the square root of the vapor temperature. As we have previously demonstrated with EIT in warm Rb and acetylene vapor confined to a 6 μm core HC-PBGF, this effect is estimated to be in the range of 15–50 MHz [4,17,34]. Transit-time

*Current address: Steacie Institute for Molecular Sciences, National Research Council of Canada, Ottawa, Ontario, Canada K1A 0R5; e-mail: aaron.slepkov@nrc.ca

broadening occurs when fast-moving particles rapidly traverse the light mode, limiting the photonic interactions to time scales shorter than the natural lifetimes of the system. In the reference frame of the particles, the light appears to be modulated at the transit-time frequency, and, thus, adds new Fourier components that manifest as broadening in the homogeneous linewidth [41]. In the case of hollow-core waveguides, transit-time and wall-collision broadening occur simultaneously, since the light mode only partially fills the core. However, in evanescent interaction geometries—such as for the tapered optical-fiber experiments of Spillane *et al.* [6]—transit-time broadening occurs separately from wall-collision broadening. In this case, where the evanescent light mode is only a few hundred nanometers wide but the vapor is essentially unbounded, transit-time effects dominate and can lead to broadening on the order of 100 MHz. Without cooling or optical trapping, transit-time broadening is unavoidable when light-matter interactions are drastically confined and can become dominant as the light-mode area is minimized [5,6]. Other factors that become relevant at the small volumes and high intensities of systems of this sort include power broadening, mode nonuniformity, and ac Stark shifts. In this paper, we present experimental evidence of the various linewidth broadening mechanisms and shifts that dominate the spectroscopy and the utility of alkali atom vapors confined to the core of an HC-PBGF and discuss their relevance and implications to light-matter interactions in other waveguiding geometries.

II. EXPERIMENTAL

In this paper, we study photonic interactions with room-temperature Rb vapor confined to the 6 μm diameter hollow core of a photonic band-gap fiber, as previously described [17,34]. We mount 45 mm long segments of commercially purchased HC-PBGF designed for guiding light in the range of 750–810 nm (Crystal Fiber, AIR-6-800) inside of an ultrahigh-vacuum steel chamber with glass windows. The chamber pressure is reduced to below 10^{-8} torr, at which point the chamber is exposed to natural Rb metal from a breakseal ampoule, and the system is heated to 45–60 °C, thereby exposing the open fiber ends to a thermal Rb vapor. Figure 1 presents a schematic of our experimental layout. Microscope objectives (New Focus, 16×) mounted outside the windows are used to couple light in and out of the fibers, with a total transmission rate of approximately 30%. The output of either fiber face can be imaged onto a CCD to assist with coupling to ensure that the light is coupled into the core mode. A milliwatt-level beam at 805 nm from a tunable cw Ti:sapphire ring laser is coupled into the fiber and is used to generate an on-demand Rb vapor inside the fiber using light-induced atomic desorption (LIAD), as discussed below. The output of a scanning diode laser tuned to span the D_1 line of Rb at 795 nm is split (90:10) and is routed to couple in a counterpropagating direction through the fiber. The stronger (10 nW–1 μW) pump beam combines with the LIAD beam at a polarizing beam cube, and is coupled through the fiber. The weaker (0.2–10 nW) signal beam is coupled through the other end of the fiber, and, using a flip mount, can also be rerouted through the optical cell without passing through the

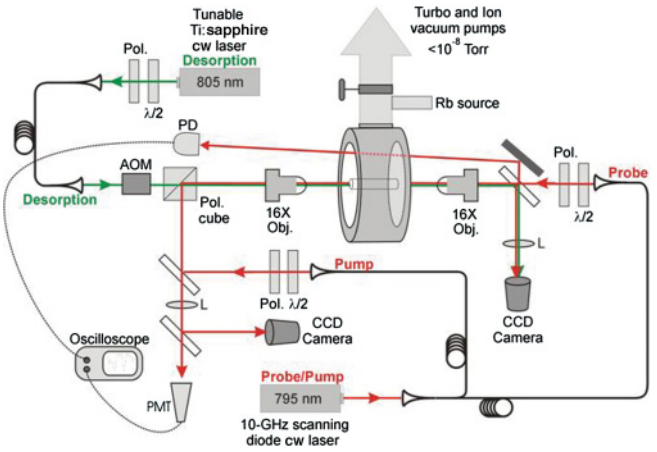

FIG. 1. (Color online) A schematic of the experimental layout: A 4.5 cm long hollow-core photonic band-gap fiber is mounted inside a steel chamber with glass windows connected to an ultrahigh-vacuum system. A 795 nm diode laser beam is scanned mode-hop free over 10 GHz and split into the pump and signal beams, which counterpropagate through the HC-PBGF. An 805 nm light-induced atomic desorption beam is mixed with the pump beam at a polarizing beam cube and is coupled into the fiber with 10× microscope objectives. An acousto-optic modulator (AOM) allows for the pulsing of the LIAD beam in order to regulate the optical depth, if needed. The coupling is monitored using a charge-coupled device (CCD) camera. The probe beam can alternately be passed through the cell and can be detected by a photodiode to monitor the ambient cell Rb density. The coupled probe light is detected with photomultiplier tube (PMT). lens (L); photodiode (PD); polarizer (Pol); polarizing beam cube (Pol cube); half-wave plate ($\lambda/2$).

fiber to serve as a monitoring beam for the ambient Rb-vapor density. Once sufficient and repeatable amounts of Rb vapor can be generated in the fiber using LIAD, the cell and the Rb ampoule can be returned to room temperature, and the fiber can be used for weeks without the need for reloading Rb [33].

Rb atoms adsorb onto the inside surface of the fiber but do not establish a stable thermal vapor in the fiber. Instead, a controlled, on-demand, vapor of Rb is generated by applying an off-resonance LIAD beam [42]. Once the fiber is sufficiently loaded with Rb to show a strong desorption with optical depths greater than ~100, the Rb redistributes in the fiber over a period of minutes to hours and can be redesorbed. Once redesorbed, the amount of Rb vapor accessible optically may be depleted, and the Rb is left to redistribute in the fiber. We typically allow a 2 to 3 h redistribution period. Details of this desorption process have been recently described in Ref. [34].

For saturable-absorption spectroscopy, we repeatedly scan the frequency of the diode laser at 100 Hz across the D_1 line and counterpropagate the pump and signal beams. We vary the coupled laser power between 5 and 30 nW for the signal and 10 and 1000 nW for the pump. The probe beam is passed through narrow-band 795 nm filters (TFI 795MC10) and is detected using a PMT. The output of the PMT is coupled to an oscilloscope using suitable impedance termination.

For passive slow-light experiments, we use a slightly modified experimental setup in which a 30 cm long piece of HC-PBGF traverses two UHV optical chambers, as described previously [17]. We carve short, 5 ns, pulses from the same

795 nm diode cw laser using an electro-optic modulator (EOM). This is achieved by driving the EOM (EOSPACE Model PM-OK1-10-PFU-800) with a modulated sinusoidal 10 GHz frequency from an rf generator. The cw signal is modulated by mixing with a 100 ps rise time, 5 ns duration, square pulse, ultimately creating two weak 5 ns pulses at a frequency detuned by 10 GHz on either size of the main laser frequency. Finally, a 400 MHz linewidth, 40 GHz free-spectral-range, solid-state etalon is used as a passband filter for this 5 ns probe pulse, excluding the main laser frequency and opposite sideband pulse. For the pulse-delay experiments, the etalon and the probe pulse frequency are tuned to the center of the D_1 line between the ^{85}Rb $F = 3 \rightarrow F' = 3$ and $F = 2 \rightarrow F' = 2$. The probe pulses are then coupled through the hollow-core fiber and are incident on a PMT for detection. The PMT signal passes through a transimpedance amplifier (FEMTO current amplifier, HCA-200M-20K-C) before being sent to an ultrafast (5 GHz) oscilloscope for data recording.

III. RESULTS AND DISCUSSION

A. ac Stark shifts

The use of LIAD for the generation of a dense Rb vapor inside the fiber allows for the rapid generation of extremely large optical depths in a repeatable manner. In previous work [5,22], groups have relied on a thermal atomic vapor for loading hollow-core semiconductor waveguides or TOFs [6,24], but have obtained small optical depths (ODs) of order of 1 (where OD is defined as minus the natural log of the minimum transmission through the generated vapor). The utility of an alkali vapor for slow-light applications, for example, relies on the ability to generate large optical depths [43]. This suggests that it may prove advantageous to adopt an experimental protocol that utilizes LIAD for vapor generation, and a recent report by Hendrickson *et al.* [24] has already described their need for using LIAD both to obtain Rb vapors and to maintain optical transmission in a TOF experimental system. Thus, the investigation of line-shape broadening and light shifts arising from the use of a relatively strong far detuned desorption beam is relevant for systems beyond HC-PBGF. To obtain the highest optical depth of Rb [33], we use 18–20 mW of coupled 804.5 nm LIAD light. This beam is 10.5 nm detuned from the nearest resonance of Rb (D_1 line at 795.0 nm) and is, thus, described as far detuned. For atomic systems with few-millihertz natural line shapes, 1 GHz is typically considered far detuned. However, 18 mW of light coupled into a hollow waveguide of cross-sectional area on the order of 10^{-7} cm^2, represents a light intensity of 10^8 mW/cm^2. By considering that the natural far detuned saturation intensity of the D_1 line of Rb is 4.5 mW/cm^2 [44], the intensity of our desorption beam can be as much as 8 orders of magnitude larger than this value, and, thus, can yield sizable ac Stark shifts even for 10 nm (4600 GHz) detunings. The ac Stark effect of a given detuned transition, shifts the resonant energy of each coupled level by [45],

$$\Delta v_{\text{ac Stark},i} = \frac{I}{I_{\text{sat},i}} \frac{\gamma_i^2}{8\pi\delta_i}, \tag{1}$$

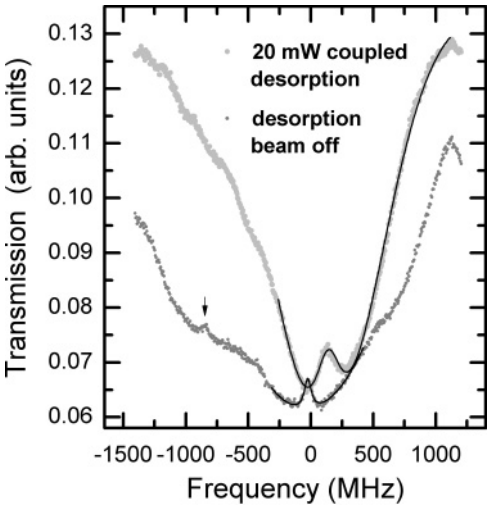

FIG. 2. Saturable-absorption spectroscopy of the ^{87}Rb $F = 1 \rightarrow F' = 2$ transition in the presence and the absence of a 20 mW desorption beam. In the presence of LIAD, a significant ac Stark shift is observed, and the line shape is seen to broaden and to distort. The arrow indicates the ^{87}Rb $F = 1 \rightarrow F' = 1$ transition. Solid lines are fits to a Lorentzian peak inside a Gaussian.

and in total shifting by

$$\Delta v_{\text{ac Stark},i} = \sum_i v_{\text{ac Stark},i}, \tag{2}$$

where I is the light-mode intensity, $I_{\text{sat},i}$ is the saturation intensity of ith transition, γ_i is the natural lifetime of the atoms in level i, and δ_i is the frequency detuning of the strong light beam from the ith transition. To calculate the Stark shift imparted on the D_1 line, we must also consider the coupling to the D_2 transition at 780 and 25 nm away.

As we have previously reported [34], when a strong desorption pulse is used to generate a large Rb density, a residual vapor can remain in the core for a second or more. This allows us to study the line shape of the saturable-absorption peak in the absence of the LIAD beam. Figure 2 shows the effects of the strong desorption beam on the line shape of the saturable-absorption signal both in the presence and in the absence of an ~20 mW desorption beam. In the presence of LIAD, the peak is both shifted and considerably broadened, as compared to that without a desorption beam. These data are well described by a simple line-shape approximation of a narrow Lorentzian subtracted inside a wider (Doppler profile) Gaussian, as seen in Fig. 2. In the presence of a 20 mW desorption pulse, the experimental ac Stark shift is approximately 180 MHz, and the line-shape full width at half maximum (FWHM) broadens nonuniformly from 35 ± 2 MHz (in the absence of LIAD) to ~150 MHz. By using Eqs. (1) and (2) and considering our use of linearly polarized light, we expect a 90 MHz ac Stark shift in total when summed over all relevant level coupling in the D_1 and D_2 lines. Thus, our experimental shift is considerably larger than would be expected from a simple calculation using average mode powers. We believe that the source of this discrepancy resides in the nonuniformity of the guided HC-PBGF mode. Typical high-resolution saturable-absorption spectroscopy experiments conducted in bulk vapor cells

require the two beams to be near-ideally counterpropagating in order to eliminate residual Doppler signals [46], and the weak signal beam is typically focused smaller within the pump beam to approximate the sampling of a uniform pump mode. Conducting such an experiment in a hollow waveguide offers guarantees that the two beams will always be in a strict counterpropagating geometry. However, this geometry also ensures that the signal and pump modes will be near-perfectly overlapped, and, thus, neither can approximate a uniform (constant power) mode. Instead, the beams propagate as approximate Gaussian-intensity modes [47].

Since the ac Stark shift is proportional to the local intensity, the shift will be strongest for atoms near the center of the light mode and weaker for atoms near the core walls. This readily produces two effects: First, the nonuniformity of the mode leads to a nonconstant Stark shift across the fiber diameter, and, thus, to significant reshaping and inhomogeneous broadening of the saturated absorption peak; second, the peak of the resulting signal is shifted considerably farther than would be expected from Eqs. (1) and (2). Both of these effects are clearly observable in the 20 mW LIAD signals shown in Fig. 2. To model the effect of a realistic core mode on the ac Stark shift of a Lorentzian resonance, we integrate the ac Stark shift as a function of a Gaussian-radial-intensity profile, as weighted by the radial density of Rb atoms ($2\pi r\, dr$ assuming uniform density). In this case, the experimental core mode is approximated by a Gaussian-intensity profile with a half-width-at-half-maximum radius of 1.0 μm that fills the majority of the hollow core without significant extent beyond the physical boundaries of the 3 μm radius core walls [47]. As seen in Fig. 3, the simulated shifts given by a uniform average power mode and by a Gaussian-core mode are very different and accurately represent the experimental peak shapes presented in Fig. 2.

We have obtained saturated absorption profiles for a series of LIAD powers ranging between 4 and 19 mW. For each desorption power, the signal is fitted as in Fig. 2, and the total shift is extracted from the peak position of the fit. As shown in

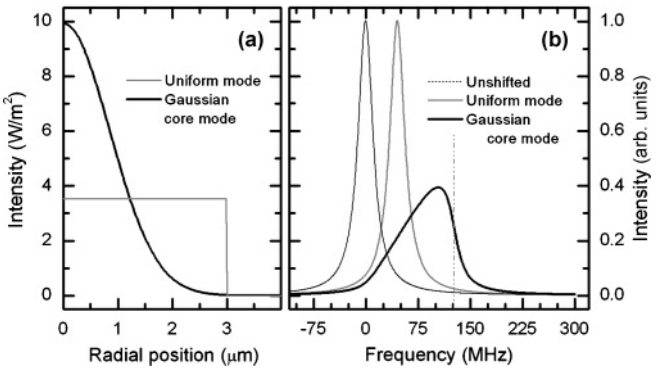

FIG. 3. The effect of guided mode nonuniformity on the ac Stark shift. (a) Radial mode profiles for 10 mW flat-top and Gaussian-core modes. (b) Simulated ac Stark shifts of a Lorentzian saturated-absorption peak by flat-top and Gaussian-core modes. The vertical dashed line represents the maximum shift experienced by the most intense component of the core mode. The nonuniformity of the core mode is also seen to broaden and to steepen the line toward higher frequencies.

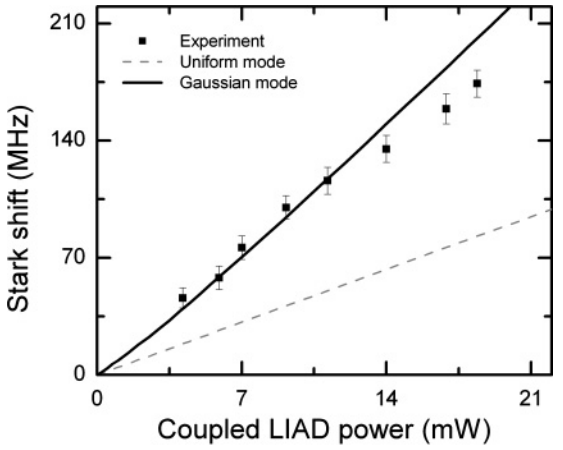

FIG. 4. ac Stark shifts as functions of desorption beam power. 30-nW and 150-nW powers were used for the counterpropagating signal and the pump beams, respectively. The experimental shifts are larger than those expected for a flat-top mode (dashed line) and are well fit by the simulated shift of a nonuniform Gaussian-guided mode (solid line).

Fig. 4, the experimental Stark shift is quasilinear and is well approximated by our nonuniform mode simulation. Overall, we find that with the intense desorption powers necessary for the generation of large Rb optical densities in hollow-core fibers, light shifts on the order of hundreds of megahertz can be induced. This represents both a shift and a broadening that are many times the natural linewidth of the transitions of interest, and the effect must, thus, be considered when using milliwatt-level desorption beams for the generation of large atomic vapor densities.

B. Power broadening and transit-time broadening

One of the main advantages of working with confined waveguiding geometries is the potential to operate in a regime where nonlinearities can be produced at extremely low powers. Power broadening becomes significant when the light intensity exceeds the saturation intensity of the medium, which, for alkali atoms confined within micrometer-sized light modes, can be as low as a few nanowatts. Molecular gases are typically weaker absorbers by several orders of magnitude, and, thus, have much higher saturation powers than alkali atoms. Typical reported saturation powers for acetylene in a 10 μm core HC-PBGF are 20–50 mW [19,20]. Significant power broadening has been reported in saturated absorption spectroscopy of molecules loaded into a hollow-core fiber [19–21,24,30]. Figure 5 presents an analysis of linewidth broadening as a function of pump power for saturable-absorption spectroscopy on the ^{87}Rb $F = 1 \rightarrow F' = 2$ transition in our system. To avoid the aforementioned broadening due to the combination of mode nonuniformity and the ac Stark shift, these data were taken with post-LIAD residual vapor, as shown in the bottom curve of Fig. 2. The power-broadening scales as

$$\Delta\nu = \gamma(1 = P/P_{\text{sat}})^{1/2}, \tag{3}$$

where $\Delta\nu$ is the experimental FWHM of the (quasi-) Lorentzian linewidth, γ represents the linewidth in the absence

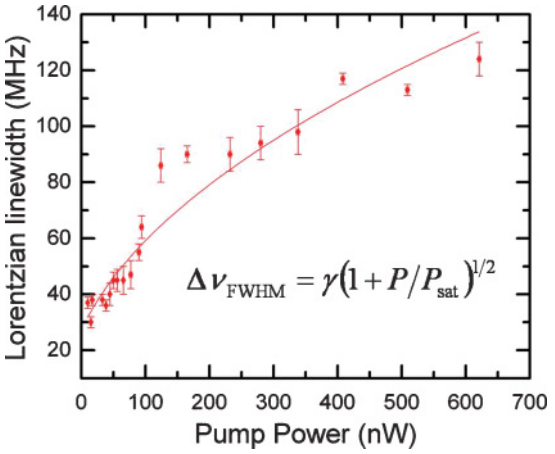

FIG. 5. (Color online) Measured power broadening of Rb atoms confined to the core of the band-gap fiber and predicted linewidth broadening as a function of pump power measured via saturable-absorption spectroscopy on the ^{87}Rb $F = 1 \rightarrow F' = 2$ transition in our system. The intercept represents the minimum linewidth available limited by transit-time broadening.

of power broadening, and P_{sat} is the saturation power of the interaction geometry [48]. Typically, γ is the natural linewidth of the medium (~5.75 MHz for the D_1 line of Rb), but, in the more general case, it is the homogeneous linewidth in the absence of light. In our case, this value represents the lower limit on the linewidth resulting from transit-time broadening, and, thus, represents an additional measurement of this effect. By fitting the data in Fig. 5 to the expression in Eq. (3) yields values of 27 ± 3 MHz and 26 ± 7 nW for the transit-time broadening and saturation power, respectively. As discussed earlier, a strict interpretation of the observed saturation power may be misleading, since as with the case of the ac Stark shift, mode nonuniformity will lead to deviations from the simple expression of Eq. (3). Nonetheless, this observed saturation power is an order of magnitude larger than that expected from the natural lifetime of Rb, yet is many orders of magnitude smaller than that observed in bulk vapor cells. It is also 6 orders of magnitude smaller than that observed for molecules in similar core-sized HC-PBGFs, as mentioned previously. This increase in saturation power is derived from the increased homogeneous linewidth from transit-time broadening. A value of 27 ± 3 MHz of transit-time broadening agrees well with our prior estimates obtained from geometric considerations and global fits to absorption spectra [34]. This value represents the narrowest line shape available for Rb atoms in a 6 μm confined geometry. As a result, most light-matter interactions in confined micro- and nanoscaled geometries will suffer this transit-time broadening. For example, hollow semiconductor waveguides, such as the ARROW architecture reported by Yang *et al.* [5] confine atoms across a similar mode area to that of standard HC-PBGF and, thus, exhibit similar linewidths and should display similar saturation powers. On the other hand, evanescent interactions with nanoscale TOF take place on considerably smaller cross-sectional scales and will, thus, yield considerably wider minimum linewidths and much larger saturation intensities. For example, the TOF system reported by Spillane *et al.* [6] experiences a transit-time broadened lifetime minimum of 110 MHz. This value corresponds to a saturation power of >300 nW. This issue will ultimately impose limitations on the spectroscopic utility of such geometries for sensing applications and resonant nonlinear optics.

C. Impact of increased linewidths on off-resonant applications

The increased homogeneous linewidths associated with effects such as transit-time broadening also strongly impact on the utility of such systems for nonresonant applications. Here, we elucidate the effect by studying its impact on the delay times generated in a passive slow-light experiment. As recently shown by Camacho *et al.* [49] when a short laser pulse is tuned between two strongly absorbing and widely spaced resonances, the amount of group delay experienced by the pulse is inversely proportional to the homogeneous linewidths, and is approximately given by

$$\tau_g = \frac{-\ln(T)}{2\pi\gamma}, \tag{4}$$

where τ_g is the pulse delay, T is the peak pulse transmission, and γ is the homogeneous linewidth of the two resonances. This approximate expression is based on the assumption that the pulse is centered between the two resonances, which are Lorentzians of equivalent strength. It is interesting to note that the achievable time delay does not depend explicitly on the frequency spacing between flanking resonances but rather indirectly via the achievable optical depth at the pulse frequency through the transmission T. For an ~2.5 ns pulse centered between the ^{85}Rb D_2 line doublet in a bulk vapor cell, Camacho *et al.* [49] showed that the time delay closely follows Eq. (4), with the expected natural linewidth of 6.07 MHz.

In Fig. 6, we present results of similar passive slow-light experiments conducted in the HC-PBGF on the ^{85}Rb D_1 line in HC-PBGF using 4.6 ns pulses. By fitting the data in Fig. 6 to Eq. (4) illustrates that the transit-time and other broadening mechanisms reduce pulse delay by a factor of 10 in comparison to a bulk cell geometry. From the data in Fig. 6,

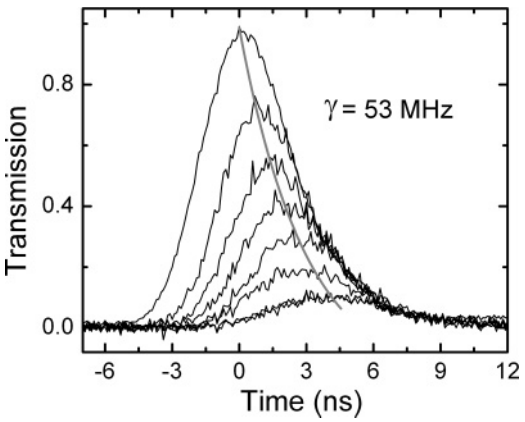

FIG. 6. Passive slow light in the center of the Rb D_1 line. Pulse delay in HC-PBGF as a function of optical depth for a 4.6 ns, 795 nm pulse centered between the ^{85}Rb $F = 2 \rightarrow F' = 2$ and $F = 3 \rightarrow F' = 3$ transitions. The solid gray line is a fit to an exponential function that estimates the experimentally accessed homogeneous linewidth (see text).

we estimate a Lorentzian linewidth of 53 ± 20 MHz, which is slightly broader than that estimated by the more direct means discussed previously. Deviations from ideal behavior are due to the fact that the D_1 line is not composed of an isolated doublet, but rather contains four lines of different strengths, and that as shown previously [33], at this spectral location in the center of the D_1 line, the line shape follows a Voigt profile with a nonnegligible Doppler-broadened Gaussian component. Nonetheless, comparing our pulse-delay results to those reported for bulk cells [45,50] clearly demonstrates that the modifications to the spectroscopic line shapes of atoms confined in waveguiding geometries can also be important for highly nonresonant light-matter interactions.

IV. SUMMARY

We have performed a detailed spectroscopic study of light-matter interactions with warm alkali atoms confined to the 6 μm core of a hollow-core photonic band-gap fiber. Using saturable-absorption spectroscopy, we show, for the first time, the various line-shape shifts, broadening, and distortions that take place in such a system, and further discuss the relevance of these findings to similar micrometer-scale light-atom interaction geometries. We find that the use of a strong desorption beam for the creation of an atomic vapor leads to strong ac Stark shifts, even when detuned off-resonance by many thousands of gigahertz. Furthermore, the Gaussian-like spatial profile of the light modes in these waveguides leads to a distribution of ac Stark shifts and, thus, to considerable line-shape broadening and distortion. These effects can be mitigated by performing the interaction of interest immediately after the desorption beam is turned off. In addition, the effects of transit-time broadening play an important role even for applications based on nonresonant interactions such as slow light and pulse delays.

ACKNOWLEDGMENTS

We gratefully acknowledge financial support from the Centre for Nanoscale Systems, the Air Force Office of Scientific Research, and the Defense Advanced Research Projects Agency under the Slow-Light program.

[1] M. Bajcsy, S. Hofferberth, V. Balic, T. Peyronel, M. Hafezi, A. S. Zibrov, V. Vuletic, and M. D. Lukin, Phys. Rev. Lett. **102**, 203902 (2009).
[2] P. Londero, V. Venkataraman, A. R. Bhagwat, A. D. Slepkov, and A. L. Gaeta, Phys. Rev. Lett. **103**, 043602 (2009).
[3] F. Benabid, J. C. Knight, G. Antonopoulos, and P. St. J. Russell, Science **298**, 399 (2002).
[4] S. Ghosh, J. E. Sharping, D. G. Ouzounov, and A. L. Gaeta, Phys. Rev. Lett. **94**, 093902 (2005).
[5] W. G. Yang, D. B. Conkey, B. Wu, D. L. Yin, A. R. Hawkins, and H. Schmidt, Nature Photon. **1**, 331 (2007).
[6] S. M. Spillane, G. S. Pati, K. Salit, M. Hall, P. Kumar, R. G. Beausoleil, and M. S. Shahriar, Phys. Rev. Lett. **100**, 233602 (2008).
[7] M. Wilzbach, D. Heine, S. Groth, X. Liu, T. Raub, B. Hessmo, and J. Schmiedmayer, Opt. Lett. **34**, 259 (2009).
[8] N. Gayraud, L. W. Kornaszewski, J. M. Stone, J. C. Knight, D. T. Reid, D. P. Hand, and W. N. MacPherson, Appl. Opt. **47**, 1269 (2008).
[9] F. Couny and F. Benabid, J. Opt. A, Pure Appl. Opt. **11**, 103002 (2009).
[10] S. Knappe, V. Velichansky, H. G. Robinson, J. Kitching, and L. Hollberg, Rev. Sci. Instrum. **74**, 3142 (2003).
[11] K. Knabe, W. Shun, J. K. Lim, K. A. Tillman, P. S. Light, F. Couny, N. Wheeler, R. Thapa, A. M. Jones, J. W. Nicholson, B. R. Washburn, F. Benabid, and K. L. Corwin, Opt. Express **17**, 16017 (2009).
[12] D. A. Braje, V. Balic, G. Y. Yin, and S. E. Harris, Phys. Rev. A **68**, 041801(R) (2003).
[13] A. M. C. Dawes, L. Illing, S. M. Clark, and D. J. Gauthier, Science **308**, 672 (2005).
[14] D. F. Phillips, A. Fleischhauer, A. Mair, R. L. Walsworth, and M. D. Lukin, Phys. Rev. Lett. **86**, 783 (2001).
[15] R. M. Camacho, P. K. Vudyasetu, and J. C. Howell, Nature Photon. **3**, 103 (2009).
[16] D. G. Ouzounov, F. R. Ahmad, D. Müller, N. Venkataraman, M. T. Gallagher, M. G. Thomas, J. Silcox, K. W. Koch, and A. L. Gaeta, Science **301**, 1702 (2003).
[17] S. Ghosh, A. R. Bhagwat, C. K. Renshaw, S. Goh, A. L. Gaeta, and B. J. Kirby, Phys. Rev. Lett. **97**, 023603 (2006).
[18] F. Benabid, P. S. Light, F. Couny, and P. St. J. Russell, Opt. Express **13**, 5694 (2005).
[19] J. Henningsen, J. Hald, and J. C. Petersen, Opt. Express **13**, 10475 (2005).
[20] R. Thapa, K. Knabe, M. Faheem, A. Naweed, O. L. Weaver, and K. L. Corwin, Opt. Lett. **31**, 2489 (2006).
[21] A. M. Cubillas, J. Hald, and J. C. Petersen, Opt. Express **16**, 3976 (2008).
[22] B. Wu, J. F. Hulbert, A. R. Hawkins, and H. Schmidt, J. Lightwave Technol. **26**, 3727 (2008).
[23] J. T. Robinson, L. Chen, and M. Lipson, Opt. Express **16**, 4296 (2008).
[24] S. M. Hendrickson, T. B. Pittman, and J. D. Franson, J. Opt. Soc. Am. B **26**, 267 (2009).
[25] M. Trupke, E. A. Hinds, S. Eriksson, E. A. Curtis, Z. Moktadir, E. Kukharenka, and M. Kraft, Appl. Phys. Lett. **87**, 211106 (2005).
[26] E. A. Hinds, M. Trupke, B. Darquié, J. Goldwin, and G. Dutier, in *Proceedings of the 18th International Conference On Laser Spectroscopy (ICOLS)*, edited by L. Hollberg, J. Bergquist, and M. Kasevich (World Scientific, Singapore, 2008), pp. 272–282.
[27] T. Aoki, B. Dayan, E. Wilcut, W. P. Bowen, A. S. Parkins, T. J. Kippenberg, K. J. Vahala, and H. J. Kimble, Nature (London) **443**, 671 (2006).
[28] B. Dayan, A. S. Parkins, T. Aoki, E. P. Ostby, K. J. Vahala, and H. J. Kimble, Science **319**, 1062 (2008).

[29] A. R. Bhagwat and A. L. Gaeta, Opt. Express **16**, 5035 (2008).
[30] S. Knappe, V. Velichansky, H. G. Robinson, J. Kitching, and L. Hollberg, Rev. Sci. Instrum. **74**, 3142 (2003).
[31] J. Hald, J. C. Petersen, and J. Henningsen, Phys. Rev. Lett. **98**, 213902 (2007)
[32] P. S. Light, F. Benabid, F. Couny, M. Maric, and A. N. Luiten, Opt. Lett. **32**, 1323 (2007).
[33] F. Benabid, F. Couny, J. C. Knight, T. A. Birks, and P. St. J. Russell, Nature (London) **434**, 488 (2005).
[34] A. D. Slepkov, A. R. Bhagwat, V. Venkataraman, P. Londero, and A. L. Gaeta, Opt. Express **16**, 18976 (2008).
[35] A. R. Bhagwat, A. D. Slepkov, V. Venkataraman, P. Londero, and A. L. Gaeta, Phys. Rev. A **79**, 063809 (2009).
[36] C. K. Carniglia, L. Mandel, and K. H. Drexhage, J. Opt. Soc. Am. **62**, 479 (1972).
[37] T. Baehr-Jones, M. Hochberg, C. Walker, and A. Scherer, Appl. Phys. Lett. **86**, 081101 (2005).
[38] J. Henningsen and J. Hald, Appl. Opt. **47**, 2790 (2008).
[39] K.-J. Boller, A. Imamolu, and S. E. Harris, Phys. Rev. Lett. **66**, 2593 (1991).
[40] D. J. Fulton, S. Shepherd, R. R. Moseley, B. D. Sinclair, and M. H. Dunn, Phys. Rev. A **52**, 2302 (1995).
[41] W. Demtröder, *Laser Spectroscopy* (Springer-Verlag, Berlin, 1973).
[42] A. Gozzini, F. Mango, J. H. Xu, G. Alzetta, F. Maccarrone, and R. A. Bernheim, Nuovo Cimento D **15**, 709 (1993).
[43] D. Lukin and A. Imamoğlu, Nature (London) **413**, 273 (2001).
[44] D. A. Steck, ^{87}Rb and ^{85}RB D_1 line data, [http://steck.us/alkalidata/] (2001).
[45] K. Shimoda, ed., *High-Resolution Laser Spectroscopy*, (Springer-Verlag, New York, 1976).
[46] S. Haroche and F. Hartmann, Phys. Rev. A **6**, 1280 (1972).
[47] P. St. J. Russell, J. Lightwave Technol. **24**, 4729 (2006).
[48] M. L. Citron, H. R. Gray, C. W. Gabel, and C. R. Stroud Jr., Phys. Rev. A **16**, 1507 (1977).
[49] R. M. Camacho, M. V. Pack, and J. C. Howell, Phys. Rev. A **73**, 063812 (2006).
[50] H. Tanaka, H. Niwa, K. Hayami, S. Furue, K. Nakayama, T. Kohmoto, M. Kunitomo, and Y. Fukuda, Phys. Rev. A **68**, 053801 (2003).